COLOR SEPARATION OF GALAXY TYPES IN THE SLOAN DIGITAL SKY SURVEY IMAGING DATA

Iskra Strateva,[1] Željko Ivezić,[1] Gillian R. Knapp,[1] Vijay K. Narayanan,[1] Michael A. Strauss,[1] James E. Gunn,[1] Robert H. Lupton,[1] David Schlegel,[1] Neta A. Bahcall,[1] Jon Brinkmann,[2] Robert J. Brunner,[3] Tamás Budavári,[4,5] István Csabai,[4,5] Francisco Javier Castander,[6] Mamoru Doi,[7] Masataka Fukugita,[8,9] Zsuzsanna Győry,[4,5] Masaru Hamabe,[7] Greg Hennessy,[10] Takashi Ichikawa,[11] Peter Z. Kunszt,[4] Don Q. Lamb,[6] Timothy A. McKay,[12] Sadanori Okamura,[7] Judith Racusin,[12] Maki Sekiguchi,[8] Donald P. Schneider,[13] Kazuhiro Shimasaku,[7] AND Donald York[6]

ABSTRACT

We study the optical colors of 147,920 galaxies brighter than $g^* = 21$, observed in five bands by the Sloan Digital Sky Survey (SDSS) over ~ 100 deg^2 of high Galactic latitude sky along the celestial equator. The distribution of galaxies in the $g^* - r^*$ versus $u^* - g^*$ color-color diagram is strongly bimodal, with an optimal color separator of $u^* - r^* = 2.22$. We use visual morphology and spectral classification of subsamples of 287 and 500 galaxies, respectively, to show that the two peaks correspond roughly to early- (E, S0, and Sa) and late-type (Sb, Sc, and Irr) galaxies, as expected from their different stellar populations. We also find that the colors of galaxies are correlated with their radial profiles, as measured by the concentration index and by the likelihoods of exponential and de Vaucouleurs' profile fits. While it is well known that late-type galaxies are bluer than early-type galaxies, this is the first detection of a local minimum in their color distribution. In all SDSS bands, the counts versus apparent magnitude relations for the two color types are significantly different and demonstrate that the fraction of blue galaxies increases toward the faint end.

Key words: galaxies: fundamental parameters

1. INTRODUCTION

It has been known at least since the late 1930s that colors of galaxies reflect their dominant stellar populations and thus correlate with morphology (Humason 1936; Hubble 1936). Morgan & Mayall (1957) examined the spectra of 47 nearby galaxies and found that stellar systems with spectra dominated by A, A + F, and F stars are exclusively classified as Sc and Irr morphologically, F + G dominated stellar systems correspond to Sb galaxies, and the K stellar systems are a mix of predominantly early-type (E, S0, and Sa) galaxies, with a sizeable fraction of Sb spirals. De Vaucouleurs (1961) used a sample of 148 galaxies to establish the dependence of galaxy color on morphological type. Since then,

studies of the color distribution of galaxies have helped reveal their dominant stellar populations and star formation histories. Typical studies of galaxy colors in recent years have been based on samples of ~ 1000 galaxies. Fioc & Rocca-Volmerange (1999) used optical and near-infrared colors of 1000 galaxies to establish relations between the colors, morphological types, inclinations or shapes, and the intrinsic luminosities of galaxies. Ferreras et al. (1999) used color-magnitude and color-color analysis of *Hubble Space Telescope* photometry of ~ 1000 galaxies to infer the existence of nonnegligible star formation in elliptical galaxies and bulges at medium redshift ($z \sim 0.2$). Brown, Webster, & Boyle (2000) studied the dependence of clustering of galaxies on color. They used a catalog of $\sim 4 \times 10^5$ galaxies and selection rules based on synthetic colors given by Fukugita, Shimasaku, & Ichikawa (1995) and found that the galaxy correlation function is strongly dependent on color, with red galaxies more strongly clustered than blue galaxies by a factor of $\gtrsim 5$ at small scales.

The Sloan Digital Sky Survey (hereafter SDSS; York et al. 2000) is generating accurate photometry for an unprecedentedly large and uniform sample of galaxies, enabling us to expand galaxy color studies and extend them in new directions. The SDSS is a digital photometric and spectroscopic survey that will cover one-quarter of the celestial sphere toward the northern Galactic cap and produce a smaller area (~ 225 deg^2) but much deeper survey toward the southern Galactic cap. The photometric astrometric mosaic camera (Gunn et al. 1998; see also Project Book § 4,[14] The Photometric Camera) images the sky by scanning along great circles at the sidereal rate. The flux densities of detected objects are measured almost

[1] Princeton University Observatory, Peyton Hall, Princeton, NJ 08544.

[2] Apache Point Observatory, P.O. Box 59, Sunspot, NM 88349-0059.

[3] Department of Astronomy, MS105-24, California Institute of Technology, 1201 East California Boulevard, Pasadena, CA 91125.

[4] Department of Physics and Astronomy, Johns Hopkins University, 3701 San Martin Drive, Baltimore, MD 21218.

[5] Department of Physics, Eötvös University, Budapest, Pf. 32, Hungary, H-1518.

[6] University of Chicago, Astronomy and Astrophysics Center, 5640 South Ellis Avenue, Chicago, IL 60637.

[7] Department of Astronomy and Research Center for the Early Universe, School of Science, University of Tokyo, Hongo, Bunkyo, Tokyo, 113-0033 Japan.

[8] Institute for Cosmic Ray Research, University of Tokyo, 3-2-1 Midori, Tanashi, Tokyo, 188-8502 Japan.

[9] Institute for Advanced Study, Olden Lane, Princeton, NJ 08540.

[10] US Naval Observatory, 3450 Massachusetts Avenue, NW, Washington, DC 20392-5420.

[11] Astronomical Institute, Tohoku University, Aoba, Sendai, 980-8578 Japan.

[12] Department of Physics, University of Michigan, 500 East University, Ann Arbor, MI 48109.

[13] Department of Astronomy and Astrophysics, 525 Davey Laboratory, Pennsylvania State University, University Park, PA 16802.

[14] See http://www.astro.princeton.edu/PBOOK/welcome.htm.

simultaneously in five bands (u, g, r, i, and z; Fukugita et al. 1996) with effective wavelengths[15] of 3543, 4770, 6231, 7625, and 9134 Å. The telescope is also equipped with two double fiber-fed spectrographs. Fiber plug plates are individually drilled for each field to accommodate 640 optical fibers of 3" entrance diameter, which feed the spectrographs. The survey sky coverage of about π steradians (10,000 $\deg^2$) will result in photometric measurements of $\sim 5 \times 10^7$ galaxies, as well as $\sim 10^6$ moderate-resolution ($\lambda/\delta\lambda = 1800$) spectra of galaxies brighter[16] than $r_{petro} \approx 17.8$, covering the wavelength range 3800–9200 Å. The morphological information from the images currently allows robust star-galaxy separation to ~ 21.5 mag (Lupton et al. 2001; Yasuda et al. 2001).

The SDSS galaxy data have already been used in a number of studies. Blanton et al. (2001) analyze 11,275 galaxies with redshifts and photometry to calculate the galaxy luminosity function and its dependence on galaxy properties such as surface brightness, intrinsic color, and morphology. Yasuda et al. (2001) derive the galaxy number counts, and Fischer et al. (2000) measure the effect of galaxy-galaxy weak lensing. A series of papers in preparation (Zehavi et al. 2001; Tegmark et al. 2001; Dodelson et al. 2001; Szalay et al. 2001; Connolly et al. 2001) analyze in detail the clustering of galaxies in SDSS and calculate the three-dimensional power spectrum. Bernardi et al. 2001 study various scaling relationships in a sample of 9000 early-type galaxies. In a nice complementary paper to the current work, Shimasaku et al. (2001) investigate in detail the colors, effective size, and concentration parameter of SDSS galaxies, based on a sample of 456 bright objects classified visually into seven morphological types. They perform important tests on consistency of SDSS galaxy colors with those obtained from both conventional $BVRI$ photometry and synthetic colors calculated from template spectroscopic energy distributions of galaxies.

One of the scientific goals of the SDSS is to study the dependence of galaxy properties such as the luminosity function, size distribution, evolution, and large-scale distribution on morphological type. While morphological types can be assigned with some certainty to nearby well-resolved galaxies, this is not possible for the fainter and more distant galaxies imaged by SDSS. If we can find a relationship between observed color and morphological type, this relation (if fairly independent of K-corrections)

can in principle replace morphological segregation in studies of galaxy properties and distribution all the way to the limit at which we can do reliable star-galaxy separation. In this paper, we study the color distribution of a large uniform sample of 147,920 galaxies detected in SDSS commissioning data and show that the $u^* - r^*$ color distribution is bimodal, with a clear separation between the two classes down to the SDSS imaging faint limit. We describe the data samples and analyze the color distribution in § 2, followed by a discussion of the correlations between color and conventional morphological and spectral types in § 3. We present our conclusions in § 4.

2. DATA ANALYSIS

2.1. *Samples*

In the analysis of the galaxy colors we use the model magnitudes as measured by the SDSS photometric pipeline PHOTO (version 5.2; Lupton et al. 2001). The model magnitudes are calculated by fitting de Vaucouleurs and exponential models, convolved with the point-spread function (PSF), to the two-dimensional images of galaxies in the r band, and computing the total magnitude corresponding to the better fit (see the Appendix). This r-band fit is applied in all five bands, yielding galaxy colors measured through the same aperture. The estimated photometric errors are a function of magnitude: $\Delta m \approx c_1 + c_2 10^{0.2}$ mag, where the first term models the lower limit of the error due to sky subtraction and the second term models the photon statistics. Those error estimates do not include the uncertainty in the photometric calibration, which for this data is on the order of 0.03 mag. The values of the c_1 and c_2 coefficients, obtained by a linear fit for c_2 with c_1 set to the median value of the error at the bright end ($m < 16$), are given in Table 1. The photometric errors are less than 0.1 mag for $u^* \lesssim 19$, $g^* \lesssim 22$, $r^* \lesssim 21$, $i^* \lesssim 21$, and $z^* \lesssim 18$. The photometric errors at magnitudes of 16, 18, 20, 21, and 22 in all five bands are given in Table 1. The quoted photometric errors are consistent with those obtained by repeated observations. We correct the data for Galactic extinction determined from the maps given by Schlegel, Finkbeiner, & Davis (1998). Typical values for the high-latitude regions discussed in this work are $A_{r_*} = 0.05$–0.15 mag ($A_{r_*} = 0.84A_v$).

We discuss three galaxy samples, termed *photometric*, *spectroscopic*, and *morphological*. The photometric sample is a magnitude-limited ($g^* \lesssim 21$) sample of 147,920 galaxies over 101.4 $\deg^2$ of SDSS imaging data (equatorial run 756) obtained on 1999 March 22. The sample includes galaxies from five of the six nonadjacent 13.5-wide strips along the celestial equator with $-1°2687 < \delta < 1°2676$ and $9^h40^m < \alpha < 15^h42^m$ (J2000.0). The photometric errors in

---

[15] We refer to the measured magnitudes in this paper as u^*, g^*, r^*, i^*, and z^* because the absolute calibration of the SDSS photometric system is still uncertain at the ~ 0.03 mag level. The SDSS filters themselves are referred to as u, g, r, i, and z. All magnitudes are given on the AB_v system (Oke & Gunn 1983). For additional discussion regarding the SDSS photometric system, see Fukugita et al. (1996) and Fan et al. (1999).

[16] For the definition of Petrosian magnitude see Blanton et al. (2001), Yasuda et al. (2001), and Strauss et al. (2001).

TABLE 1

PHOTOMETRIC ERROR COEFFICIENTS AND SAMPLE ERRORS

Band	c_1	c_2	$m = 16$	$m = 18$	$m = 20$	$m = 21$	$m = 22$
u^*......	0.021	1.3×10^{-5}	0.04	0.07	0.15	0.23	0.35
g^*......	0.002	3.6×10^{-6}	0.01	0.02	0.04	0.06	0.09
r^*......	0.008	5.3×10^{-6}	0.02	0.03	0.06	0.09	0.14
i^*......	0.002	7.0×10^{-6}	0.01	0.03	0.07	0.11	0.18
z^*......	0.006	2.0×10^{-5}	0.04	0.09	0.20	0.32	0.51

NOTE.—The $\Delta m \approx c_2 10^{0.2}$ mag fits for c_2 were obtained using ~ 5000 randomly selected galaxies from the photometric sample, with c_1 set to the median error for $m < 16$.

the $g^* \leqslant 21$ sample are typically less than 0.03 mag in g^*, r^*, and i^*, are 0.06 mag in z^*, and increase to ~ 0.2 mag in u^*. This sample is used to study the distribution of galaxies in SDSS color space.

The spectroscopic sample, used for the detailed comparison of color and spectral classification, contains 500 galaxies from a single SDSS spectroscopic plate (plate 267, obtained on 2000 February 22, consisting of 4×15 minute exposures). Of the 500 galaxies, 443 are part of the main galaxy spectroscopic sample (for more details on the galaxy spectroscopy target selection, see Strauss et al. 2001). An additional 57 galaxies are part of the luminous red galaxies sample, composed of fainter, $0.25 < z < 0.50$, ellipticals (Eisenstein et al. 2001). The galaxies in the spectroscopic sample are distributed in a circle with radius $1°49$, centered on $\alpha = 9^h 50^m$, $\delta = 0°$ (J2000.0). The photometric data for these galaxies were obtained in SDSS commissioning runs 752 (obtained on 1999 March 21) and 756. The seeing FWHM in both runs was variable between $1''$ and $2''$, with the median value around $1''5$.

The morphological sample is a subsample of 287 bright galaxies ($g^* < 16$) from the photometric sample, which we have classified by eye and which allows studies of the correlation between color and visual morphology.

2.2. Galaxy Color Distribution

The color-magnitude and color-color diagrams of galaxies in the photometric sample are presented in Figure 1. The $g^* - r^*$ versus $u^* - g^*$ color-color diagram is displayed on the left. The distribution of galaxies from the photometric sample is shown as contours. For a detailed comparison between galaxy colors in the SDSS and various other photometric systems see Fukugita et al. 1995; for mean galaxy colors in the Cousins VRI photometric system as a function of Hubble T stage, see Buta & Williams 1995. A sample of stars with $15 < u^* < 18$ extracted from the same area of the sky as the galaxy photometric sample is plotted for comparison (*dots*). The u^* magnitude limits on the stellar sample were selected to ensure a high signal-to-

noise ratio (for more details about the color distribution of stars see, e.g., Fan 1999; Finlator et al. 2000 and references therein). The galaxy distribution has two peaks, with the line connecting them almost perpendicular to lines of constant $u^* - r^*$. This suggests that the $u^* - r^*$ color is nearly optimal for separating galaxies into the two color types.

The g^* versus $u^* - r^*$ color-magnitude diagram for the photometric sample of galaxies is presented in Figure 1 (*right*). We will refer to the subsample of galaxies on the left of the dashed line as "blue" and the one on the right as "red." When plotted as a histogram, the $u^* - r^*$ color distribution has two maxima separated by a well-defined minimum. The positions of these three extrema are only weakly dependent on the sample magnitude cut. We quantify the dependence of the three extrema on the sample magnitude limit by binning the photometric sample in g^* and fitting a sum of skewed "Lorentzian" profiles[17] to the $u^* - r^*$ color distribution of the resulting subsamples. The blue and red peaks are then given by the maxima of the "Lorentzians." We define the separator between the two as the point at which the two "Lorentzians" (with areas individually normalized to unity) have the same value. Note that this is not equivalent to finding the minimum between the blue and red peaks, since the ratio of red to blue galaxies is a function of sample magnitude cut and decreases for fainter limiting magnitudes. Sample selection using g-band limiting magnitudes or redder bands guarantees a sizeable fraction of red galaxies in fainter samples. The $u^* = 22$ cut, represented by the slanted dashed line in Figure 1 (*right*), strongly decreases the number of red relative to blue galaxies at fainter magnitudes.

The fitted positions of the three extrema for six magnitude subsamples ($16 < g^* < 21$) are plotted as circles in Figure 1 (*right*) for each mean value of the g^* bin. The error bars indicate the FWHMs of the best-fit "Lorentzians."
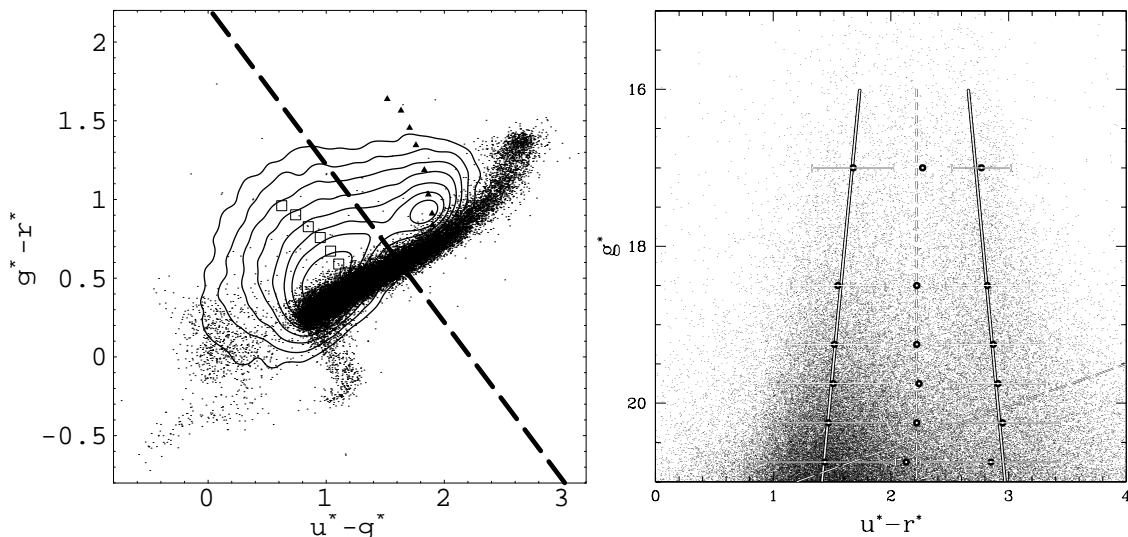
---

[17] Each "Lorentzian" is proportional to $[1 + (x - x_o)^2/(ax + b)^2]^{-1}$. The exact form of the fitted function is not critical, as long as it models the data accurately.

FIG. 1.—*Left*: Distribution of galaxies (*contours*) and stars (*dots*) in the $u^* - g^*$ vs. $g^* - r^*$ color-color diagram. The contours enclose $\sigma/4$ (20.8%) to 2σ (95.5%) of all galaxies, in steps of $\sigma/4$ (σ corresponds to the equivalent Gaussian distribution). The dashed line is the $u^* - r^* = 2.22$ separator. The evolution of spiral (*squares*) and elliptical (*triangles*) theoretical colors are given for $0 < z < 0.4$ at every 0.05 in redshift. *Right*: $u^* - r^*$ vs. g^* color-magnitude diagram of the photometric sample. Circles show positions of the red and blue peaks and the separator at each mean g^* of six subsamples (see text). Solid lines give linear regressions to the variation of each peak, while the dashed vertical line is the $u^* - r^* = 2.22$ separator. The slanted dashed line is a $u^* = 22$ cut.

The straight lines fitted through those points are $(u^* - r^*)_{blue} = 2.72 - 0.062g^*$ for the blue peak and $(u^* - r^*)_{red} = 2.17 + 0.035g^*$ for the red peak. The variation in the position of the $u^* - r^*$ separator is very small (0.1 mag) over the g^* range, showing that this criterion for separating blue and red galaxies is valid over a large range of magnitudes. The vertical line through the separator points is $u^* - r^* = 2.22$, corresponding to the mean and median of the six fits.

Two trends in the $u^* - r^*$ color distribution with fainter g^* magnitudes are visible in Figure 1 (right): (a) a shift of the blue peak toward bluer and of the red peak toward redder $u^* - r^*$ colors, quantified by the line fits given above, and (b) an overall increase of the density of blue galaxies relative to the red. The variation of the color distribution of the blue and red subsamples with apparent magnitude is due to the fact that we sample galaxies at increasing redshifts when selecting fainter magnitude cuts. The variations are caused by the color variation with increasing redshift (K-corrections and galaxy evolution) and the dependence of the sample on the galaxy number counts and luminosity function. Qualitatively, based on K-corrections alone (Fukugita et al. 1995), we expect elliptical galaxies to get redder with increasing redshift ($z \lesssim 0.3$), which is consistent with the observed slope of the $(u^* - r^*)_{red}$ line in Figure 1 (right). Based on K-corrections only, we would expect the blue galaxies to get initially redder in $u^* - r^*$ by a few tenths of a magnitude and then stay fairly constant with increasing redshift[18] for $z \lesssim 0.5$. If we include galaxy evolution through stellar population synthesis, we expect the $u^* - r^*$ color of blue galaxies to stay almost constant up to $z \sim 0.4$. The color-color diagram of Figure 1 presents the expected $u^* - g^*$ versus $g^* - r^*$ color evolution for a late spiral (squares) and an elliptical galaxy (triangles). The symbols are plotted in 0.05 redshift intervals from $z = 0$ (redder $u^* - g^*$ and bluer $g^* - r^*$) to $z = 0.4$ (bluer $u^* - g^*$ and redder $g^* - r^*$). Beyond $z \sim 0.4$, galaxies in the SDSS photometric system evolve roughly perpendicular to the $u^* - r^* = $ const cut in a $u^* - g^*$ versus $g^* - r^*$ color-color diagram, and the $u^* - r^*$ color is not a good separator. These evolutionary tracks were computed using the evolutionary synthesis model PEGASE (Fioc & Rocca-Volmerange 1997). The evolutionary prescriptions (star formation rate, initial mass function, and metallicity) were selected to reproduce the spectra of nearby galaxies at $z = 0$. The color evolution with redshift is almost parallel to $u^* - r^* = 2.22$ (dashed line on left), keeping the separator fairly constant with redshift up to $z \sim 0.4$. However, the observed $u^* - r^*$ color of the blue peak gets bluer with fainter magnitudes (see Fig. 1, right), departing from the expected evolutionary behavior of a late spiral galaxy. This departure is most likely due to an increasing degree of star-forming activity (for which the $u^* - r^*$ color is a sensitive index) with redshift, i.e., a larger number of galaxies with higher star formation activity than the modeled galaxy presented in the figure are seen at high redshift than at low redshift.

The second trend of the $u^* - r^*$ color distribution with magnitude, namely, the increase of the fraction of blue galaxies, is displayed in the four color histograms for different

g^*-magnitude bins in Figure 2 (left). For $18 < g^* < 21$, the slopes of the blue and red galaxy number counts at top right are 0.47 and 0.33, respectively, amounting to a factor of ~ 2 increase in the number ratio of blue to red galaxies. Since K-correction acts in the opposite direction (i.e., to increase the number of red galaxies), it cannot be responsible for the observed increase of blue galaxies. Moreover, this trend is present if we bin the data in r^*, i^*, or z^* bands, which sample the redder stellar populations. Two instrumental effects could cause the increase of the blue fraction as measured in apparent g^*-magnitude bins: the galaxy color distribution could get wider for fainter red galaxies, because of increased photometric errors in the u^* band (which would affect red galaxies more strongly, since they are fainter in u^*), or alternatively red galaxies could be artificially "leaking" toward blue $u^* - r^*$ colors, because the a sinh magnitudes (Lupton, Gunn, & Szalay 1999) used by SDSS cannot get fainter than a limit determined by the sky brightness in that band. We investigated both possibilities by assuming no evolution and no K-correction, i.e., the intrinsic distribution of galaxies in faint magnitude samples is similar to the observed at the bright end ($18.0 < g^* < 18.5$), and by allowing the galaxies to spread as random Gaussian deviates in the flux with fainter apparent magnitude. Using the estimates for the photometric errors in u^* and r^* as a function of magnitude given in Table 1 and $u^*(0) = 24.63$ as the zero point of the flux in the a sinh magnitude definition (see Stoughton et al. 2001), we simulated the changes in the $u^* - r^*$ color distribution with g^* magnitude due to those two effects. Figure 2 (bottom right) compares the simulated and observed fractions of red and blue galaxies, demonstrating that those effects are not sufficient to explain the change in the observed distribution. We found that the increased photometric errors cannot explain the large difference observed between the two peaks. The $u^*(0) = 24.63$ sky limit has a negligible effect for the galaxies in our photometric sample, since even the reddest are more than a magnitude brighter than this limit. Increasing the photometric errors by 50% and/or lowering the value of the sky limit to $u^*(0) = 24.00$ do not help in reconstructing the observed change in the color distribution with apparent magnitude, suggesting that we are indeed seeing an increased number of blue galaxies with fainter apparent magnitude. We conclude that the observed evolution of the $u^* - r^*$ color distribution with apparent magnitude is a real evolutionary effect, caused by the dependence of the red and blue galaxy luminosity functions or comoving volume number density on redshift. The detailed modeling needed to establish this result quantitatively is beyond the scope of this work.

Figure 3 compares the $r^* - i^*$ and $i^* - z^*$ color distributions for the two $u^* - r^*$ color-selected subsamples with $g^* < 21$. The histograms represent the data distributions, and the curves show Gaussian fits. It is evident that these two colors are quite similar for "blue" and "red" galaxies, with significant overlap between the two subsamples. The peak separation in both colors is only about 0.1–0.15 mag, much smaller than the wide $u^* - r^*$ color peak separation ($\gtrsim 1$ mag). Since the r^*, i^*, and z^* fluxes of galaxies are dominated by the old low-mass stellar populations present in all morphological types, it is indeed expected that the $r^* - i^*$ and $i^* - z^*$ colors will not show much difference for early- and late-type galaxies.

However, the fact that the $r^* - i^*$ and $i^* - z^*$ colors are not identical for the two $u^* - r^*$ color-selected galaxy types

---

[18] Here we already anticipate the identification of the blue peak with a spiral stellar population and the red peak with an elliptical; see below.
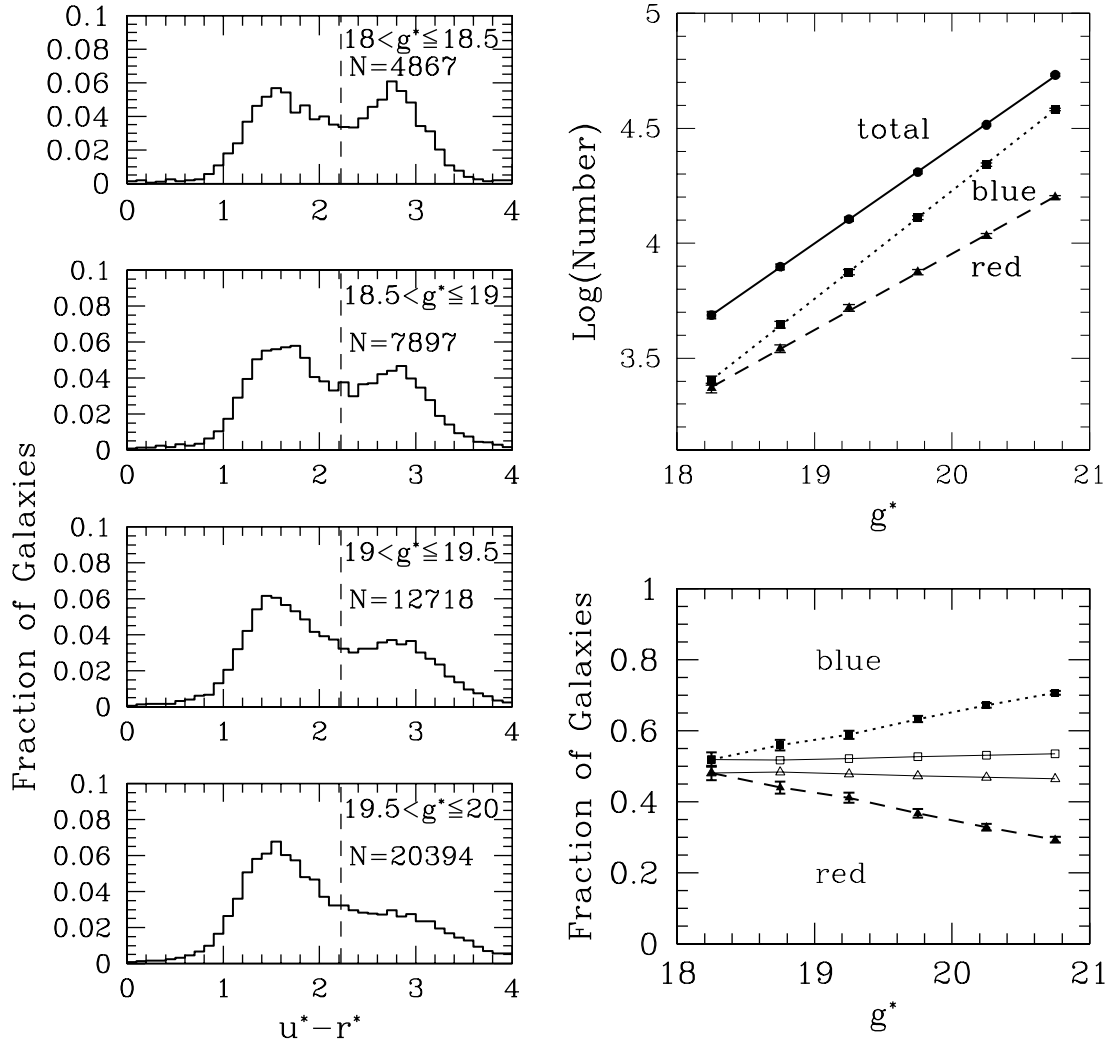
FIG. 2.—*Left*, color distribution $u^* - r^*$ as a function of g^* magnitude of the galaxy sample; *top right*, fraction of blue galaxies (*filled squares*) increasing relative to the red (*filled triangles*) for fainter g^* samples; *bottom right*, photometric errors cannot account for the dependence of the red and blue galaxy fractions on magnitude cut. The open symbols correspond to the predicted fraction (assuming only photometric errors change with magnitude), the filled symbols to the observed.
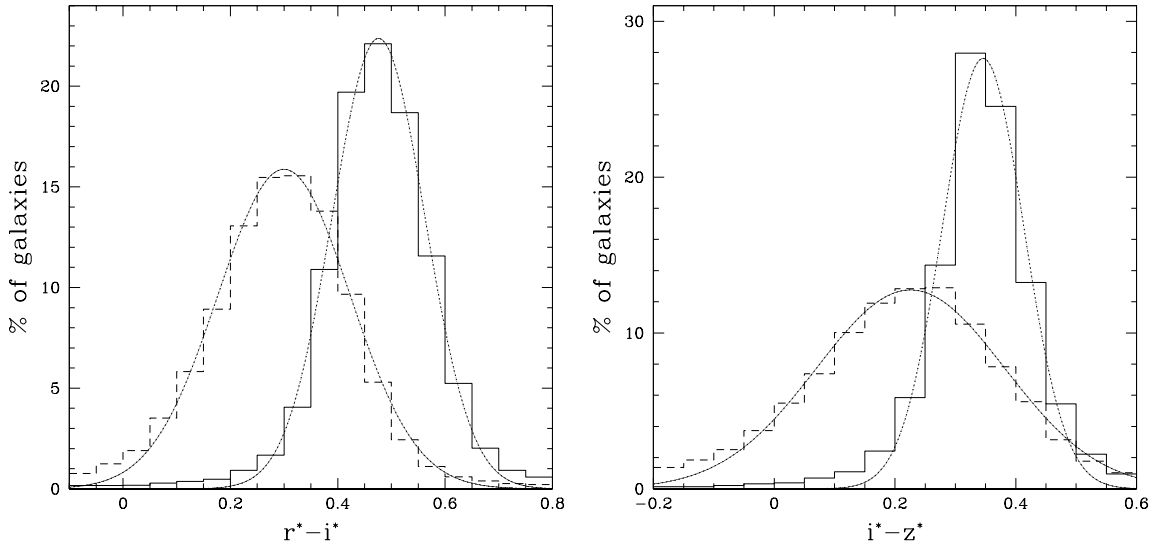
FIG. 3.—Color distributions $r^* - i^*$ and $i^* - z^*$ for two subsamples separated by their $u^* - r^*$ color (see text). The smooth curves are Gaussian fits to the data.
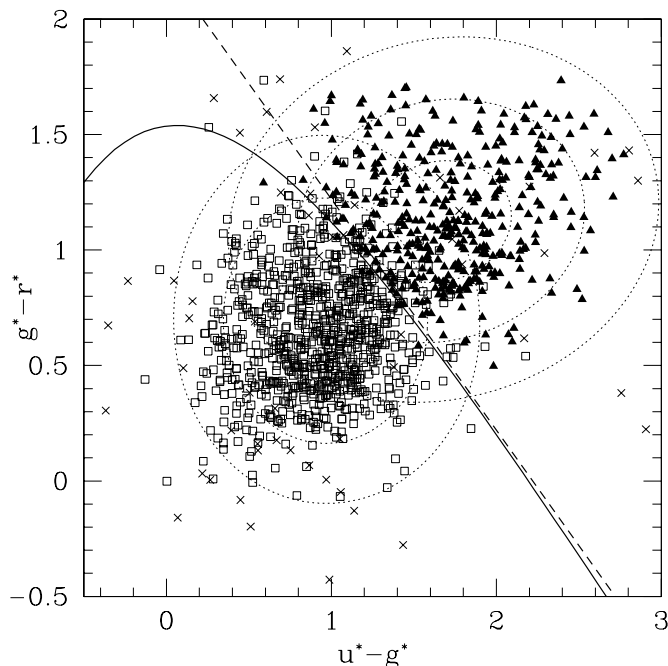
FIG. 4.—Comparison of the Bayesian cut and the u^*-r^* cut in a projection of the four-dimensional color space. Squares and triangles represent the two main classes found by the clustering algorithm (sparse sample). The crosses represent the outlier class. The dotted ellipses are the 1 σ, 2 σ, and 3 σ contours of the projected class probability ellipsoids. The diagonal dashed line is the $u^*-r^* = 2.22$ plane, which closely follows the Bayesian separator (*solid line*).

suggests that it may be possible to use this additional information to perform a better galaxy classification based on all four SDSS colors. We used the program AutoClass (Goebel et al. 1989; Cheeseman & Stutz 1996; Hanson, Stutz, & Cheesman 1999) for an unsupervised search for structure in the galaxy color distribution. AutoClass employs Bayesian probability analysis to separate a given database into classes automatically and is an efficient tool for analyzing multidimensional color diagrams. For example, Ivezić & Elitzur (2000) used AutoClass to demonstrate that the sources from the IRAS Point Source Catalog belong to four distinct classes that occupy separate regions in the four-dimensional space spanned by IRAS fluxes. We searched for self-similar classes in the galaxy color distribution by using a random subset of 25,000 galaxies from the photometric sample. While the algorithm proposed four distinct groups, most of the galaxies (82%) are included in only two classes. One of the remaining two classes represents outliers (5%), and the fourth one shows considerable overlap with one of the first two classes. We conclude that the bimodality is an excellent description of the galaxy distribution in the SDSS color space even when all four colors are used. The boundary between the two galaxy types inferred from the u^*-r^* distribution diagram is strongly supported by the AutoClass results. Figure 4 compares the Bayesian cut (*solid line*) and the u^*-r^* cut (*dashed line*). The close agreement between the unsupervised classification and the simple u^*-r^* color cut is evident.

3. COLORS AND MORPHOLOGY

3.1. *Spectroscopic and Visual Classification*

The data presented in the previous section indicate that the u^*-r^* color distribution is bimodal and that galaxies

can be divided into "blue" and "red" subsamples, as expected based on the differences in the dominant stellar populations for different morphological galaxy types (e.g., de Vaucouleurs 1961). In this section we use independent morphological classification schemes to show that the blue galaxies are indeed dominated by late types (spirals) while the red galaxies are dominated by early types (ellipticals). This is achieved by classifying a subsample of 287 galaxies by using visual appearance at the bright end ($g^* < 16$) and a fainter ($r^*_{\mathrm{petro}} < 17.8$) subsample of 500 galaxies by using spectra and comparing the results to the separation based on u^*-r^* color.

3.1.1. *Spectroscopic Classification and the u^*-r^* Color Distribution*

The 500 galaxies in the spectroscopic sample were classified by visually comparing their spectra with templates from Kennicutt's spectrophotometric atlas[19] (Kennicutt 1992a). This classification is based on the relative strengths of the H and K Ca II absorption lines (3934, 3969 Å), and the Hα (6563 Å), [N II] (6583 Å), [O II] doublet (3727 Å), Hβ (4861 Å), and [O III] doublet (4959, 5007 Å) emission lines, when present. The spectral classification did not use the equivalent widths or the fluxes of the emission lines in a quantitative way. The galaxies are separated into six types: E(0), S0(1), Sa(2), Sb(3), Sc(4), and Irr(5). Examples of the SDSS spectra for the six different classes and g^*-band images for those are presented in Figure 5. To estimate the accuracy of the classification, two of us (Strateva and Strauss) classified the galaxies independently and agreed in 410/500 cases to ± 1 class.

The correspondence between spectral classification and u^*-r^* color is shown in Figure 6 (*left*). For simplicity, the galaxies are grouped into "early" types (E, S0, and Sa; *triangles*) and "late" types (Sb, Sc, and Irr; *open squares*). Histograms of the u^*-r^* distribution for the spectroscopic sample broken into four subclasses (E/S0, Sa, Sb, and Sc/Irr) are given in Figure 7 (*left*). Practically all galaxies (97.6%) spectroscopically classified as early types have $u^*-r^* \geq 2.22$, and the remaining 3.1% are early spirals (Sa) with $u^*-r^* > 2.05$. That is, we find no examples of spectroscopically classified early-type galaxies bluer than $u^*-r^* = 2.05$. The galaxies classified spectroscopically as late type show more scatter in their colors. While 153 of the 210 late-type galaxies (73%) have $u^*-r^* < 2.22$ and over 90% (190/210) have u^*-r^* color bluer than 2.5, there are still a small number (20/210) of the spectroscopically late galaxies with $2.5 < u^*-r^* < 3.0$ and presumably low star formation rate and/or internal reddening (the images for the majority of these are consistent with either face–on spirals or ellipticals).

Kochaneck, Pahre, & Falco (2000) caution that spectroscopic classification based on fixed small apertures will systematically misclassify large angular diameter, late-type galaxies as early types, since their spectra sample mainly the bulge. Indeed 475 out of the 500 galaxies in our spectroscopic sample have more than 50% of their light outside the 3″ SDSS diameter fibers. We inspected visually the 121 galaxies among those 475 that have early-type spectra and found that 29 show a visual class later than their spectral

---

[19] Another approach to spectral classification is to search for structure in the distribution of various parameters, e.g., the expansion coefficients from the Principal Component Analysis. This is beyond the scope of this communication and will be attempted in a separate publication.
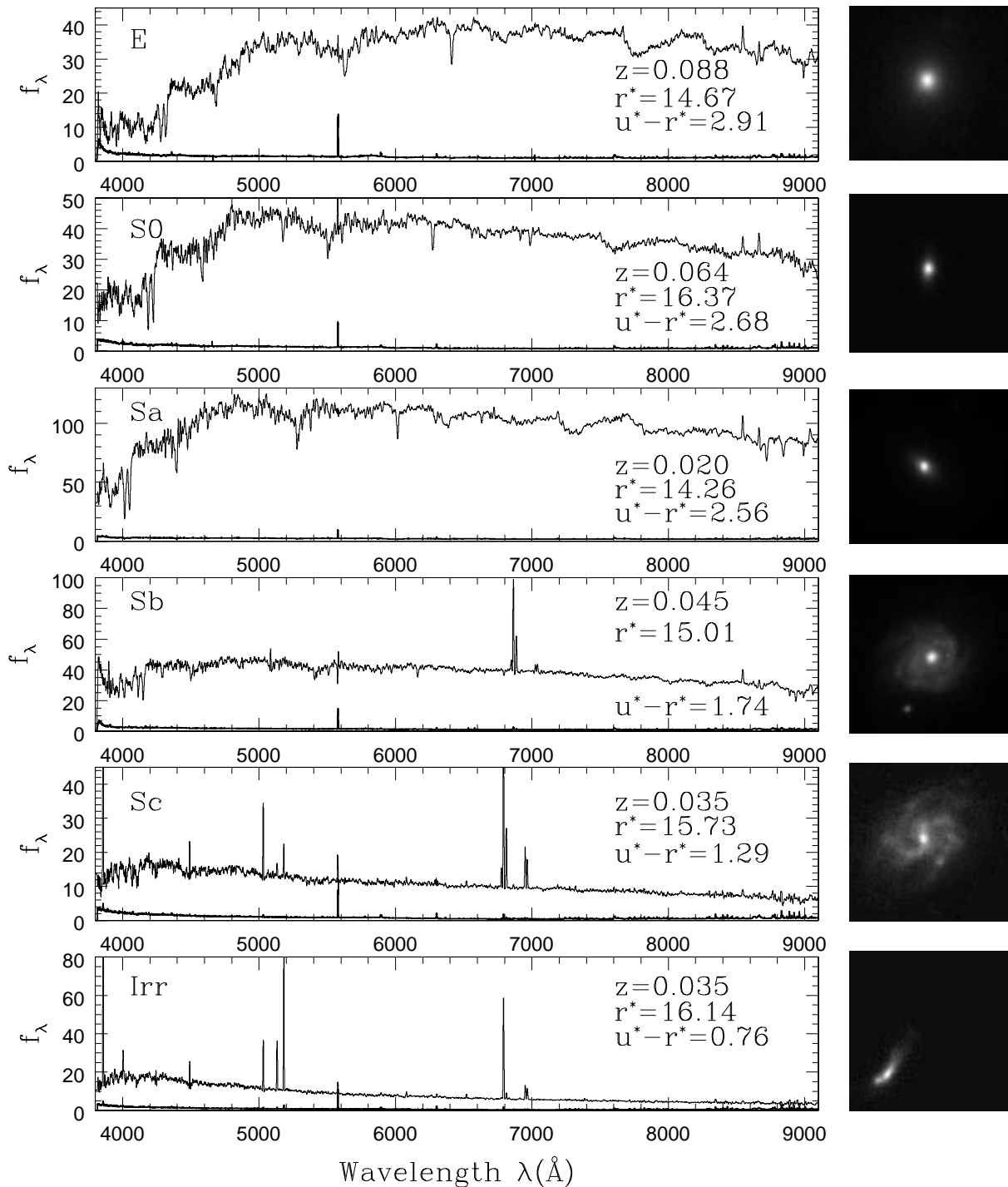
Fig. 5.—Six galaxies from the spectroscopic sample representative of the different classes and their corresponding g^*-band images. The spectra are smoothed over 5 Å, and the lower curve represents the noise in each spectrum. Each image is 40 arcsec^2.

class (15/29 visually Sa/Sb galaxies show E/S0 spectra, and 14/29 S0/Sa galaxies show E/S0 spectra), suggesting that the misclassification due to this effect is about 6%.

3.1.2. Visual Classification and the u^*-r^* Color Distribution

The visual classification is based on the optical appearance in the g^* band, which is the closest of the SDSS bands to the standard B band used for classification. We classified the 287 bright galaxies ($g^* < 16$) from the morphological sample into the same six types as in the spectroscopic sample: E(0), S0(1), Sa(2), Sb(3), Sc(4), and Irr(5). The classi-

fication was verified for 34 of those galaxies for which morphological types were found in the NASA/IPAC Extragalactic Database (NED)[20] and was found to be accurate to ± 1 class.

Figure 6 (right) presents the visually classified galaxies separated into early and late types as points over the photometric sample given in contours. Figure 7 (right) presents u^*-r^* histograms for four individual subclasses (E/S0, Sa, Sb, and Sc/Irr). Of the 117 galaxies visually classified as E,

---

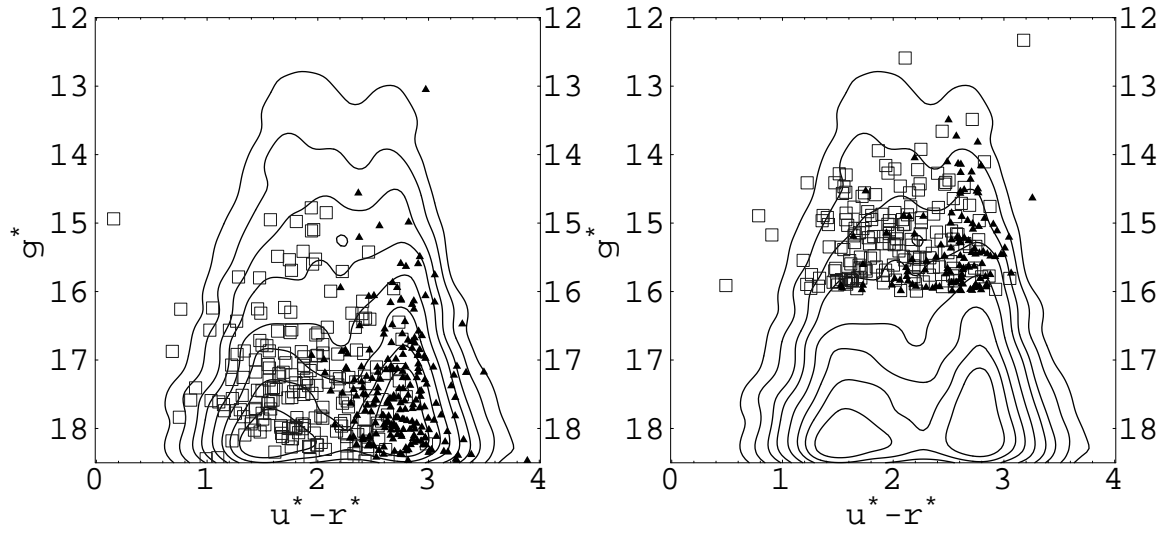[20] See http://nedwww.ipac.caltech.edu/index.html.

FIG. 6.—Bimodality in the photometric galaxy sample (*contours*) corresponds to early (*triangles*) and late (*squares*) types of galaxies. The 500 galaxies at left are classified spectroscopically; the 287 bright galaxies at right are classified by visual inspection of images.
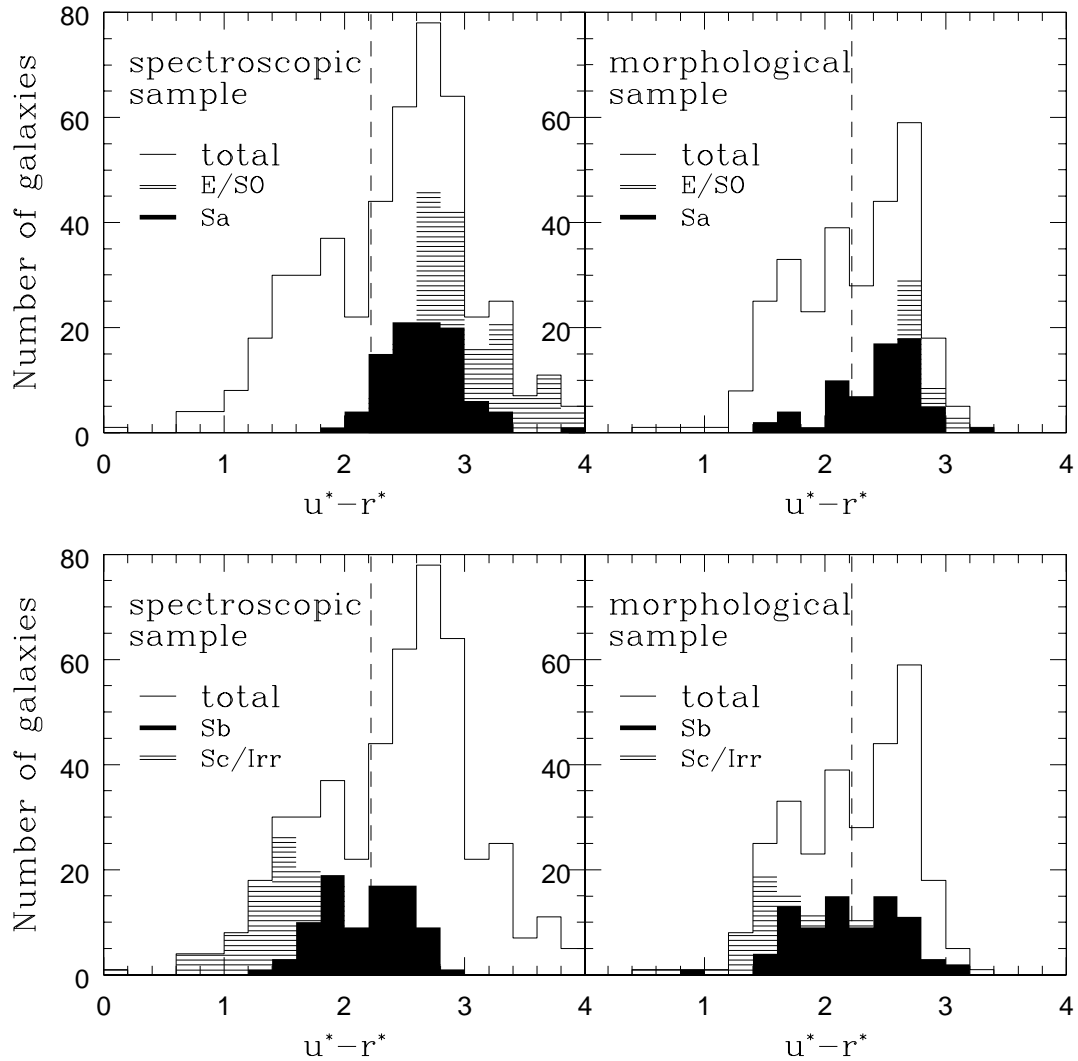

FIG. 7.—*Left*, Spectroscopic classification and $u^* - r^*$ color; *right*, morphological classification and $u^* - r^*$ color; *top*, histograms of early-type galaxies (E/S0 or Sa); *bottom*, those for late types (Sb or Sc/Irr).

SO or Sa, 80% have u^*-r^* colors redder than 2.22, consistent with being early-type galaxies. Of the 170 galaxies visually classified as Sb, Sc or Irr, 112 (66%) have colors bluer than $u^*-r^* = 2.22$, consistent with being late-type galaxies. Another 16% have colors bluer than $u^*-r^* = 2.5$, while the remaining 18% (30/170 galaxies) have colors in the range $2.5 < u^*-r^* < 3.2$ (the reddest spiral in this sample is NGC 4666, a dusty SABc LINER galaxy, in Fig. 6 [*top right*] with a $B-V$ color of 0.8 from RC2).

3.2. *Other Parameters Sensitive to Morphology*

The SDSS photometric pipeline calculates a number of global morphological parameters for every object. These include the likelihoods of the best-fit exponential or de Vaucouleurs' profiles, the "texture" parameter, and the concentration index.[21] "Texture" measures the bilateral asymmetry of an object, but it was found to be poorly correlated with galaxy type in its current implementation for both visually and spectroscopically classified galaxies and will not be considered further. Profile probabilities and concentration index both correlate well with morphology. See the Appendix for more details about the computation of these parameters.

Using the exponential (P_{exp}) and de Vaucouleurs' (P_{deV}) profile likelihoods, early-type galaxies (E, S0, and Sa) can be selected by requiring $P_{\mathrm{deV}} > P_{\mathrm{exp}}$, and late types (Sb, Sc, and Irr) by requiring $P_{\mathrm{exp}} > P_{\mathrm{deV}}$, where both likelihoods are calculated in the r band. The profile likelihood criterion is not a good discriminator at very bright magnitudes, $g^* < 16$ (see the Appendix). A similar conclusion was reached by Shimasaku et al., based on a sample of 456 bright galaxies. The basic reason for the poor performance of profile likelihoods at the bright end is the version of PHOTO pipeline used in reducing this data, which bases the profile fits on the inner profiles of galaxies, thus assigning higher likelihoods of de Vaucouleurs fits to large nearby

spirals. In the fainter spectroscopic sample used here this effect is negligible. The correspondence between the profile likelihood classification and u^*-r^* color is illustrated in Figure 8 (*left*), based on the spectroscopic sample. The histogram of galaxies with $P_{\mathrm{deV}} > P_{\mathrm{exp}}$ follows the distribution of red galaxies ($u^*-r^* \geqslant 2.22$), while the histogram of galaxies with $P_{\mathrm{exp}} > P_{\mathrm{deV}}$ follows the distribution of blue galaxies.

The concentration index, defined as the ratio of the radii containing 90% and 50% of the Petrosian r galaxy light, $C \equiv r_{p90}/r_{p50}$, also correlates with galaxy type. Centrally concentrated ellipticals are expected to have larger concentration indices than spirals. For a classical de Vaucouleurs profile $I_E(r) = I_e\,e^{-7.67[(r/r_e)^{1/4}-1]}$, the concentration index is ~ 5.5, while the exponential disks of spirals ($I_S(r) = I_S\,e^{-r/r_s}$) have concentration index ~ 2.3. Both estimates correspond to the seeing-free case; the observed values are somewhat lower. The dependence of concentration index on morphological type found in our spectroscopic and morphological samples is weak, with large scatter in C for each morphological type. The linear correlation coefficients are 0.4 and 0.7 for the spectroscopic and morphological samples, respectively, with the probability of random samples of those sizes giving the above correlation coefficients $\sim 10^{-16}$. The small correlation coefficients and the large scatter indicate that the concentration index is not a robust morphological separator, except in a very crude sense: it can be used to separate early- (E, S0, and Sa) from late-type (Sb, Sc, and Irr) galaxies. Shimasaku et al. (2001) support the use of the concentration index as a morphological separator, while noting the large uncertainty (± 1.5 class in their seven morphological types system from E to Irr galaxies) and cautioning that the concentration index cannot be used to create a pure E/S0 sample, free of Sa contamination.

Depending on whether the completeness or reliability of a subsample of a given type is to be maximized, a different concentration index separator has to be adopted. We define the *reliability* of classification as the fraction of galaxies
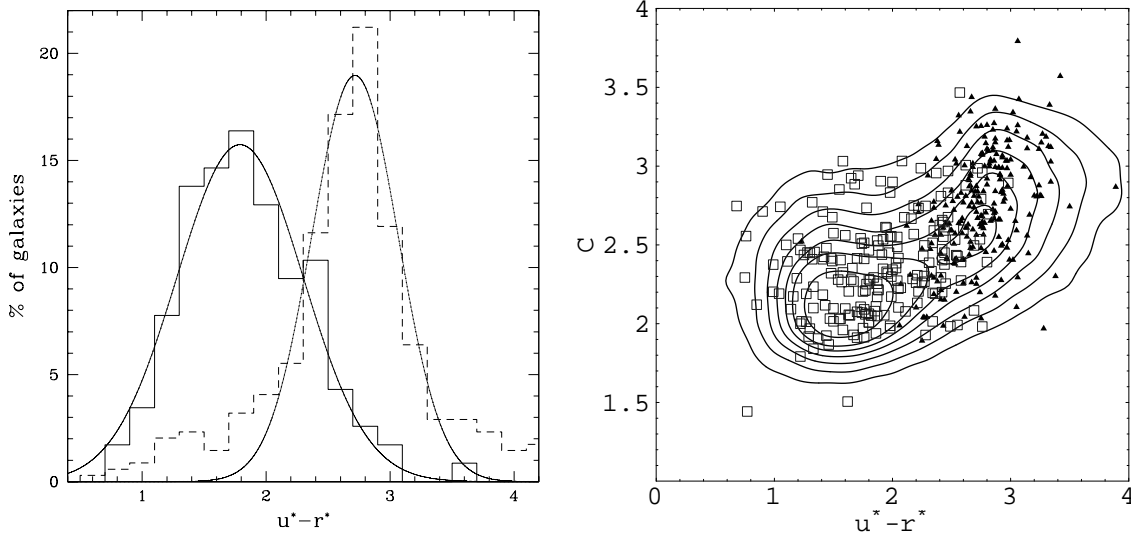
---

[21] A separate two-dimensional bulge-disk decomposition code that allows for a Sérsic bulge, exponential disk, and a bar is being developed.

FIG. 8.—Correlation of u^*-r^* color with profile likelihoods and concentration index. *Left*: Spectroscopic galaxy sample u^*-r^* histograms separated into objects with $P_{\mathrm{deV}} > P_{\mathrm{exp}}$ (early type; *dashed lines*) and $P_{\mathrm{deV}} < P_{\mathrm{exp}}$ (late type; *solid lines*), showing the same bimodality as does galaxy u^*-r^* color. Gaussian fits to the two histograms are given as a guide to the eye. *Right*: Concentration index vs. u^*-r^*. The photometric sample is given as contours enclosing $\sigma/4$ (20.8%) to $2\,\sigma$ (95.5%) of all galaxies with $g^* \leqslant 20$, in steps of $\sigma/4$ as in Fig. 1. The triangles correspond to early spectroscopic sample galaxies (E, S0, and Sa) and the squares to late spectroscopic sample galaxies (Sb, Sc, and Irr); early-type galaxies have higher concentration index than late types.

from the selected subsample that are correctly classified. For example, the $u^* - r^* \geqslant 2.22$ early-type (E, S0, and Sa) color selection criterion selects 343 galaxies from the spectroscopic sample, 284 of which have spectra consistent with an E, S0, or Sa galaxy. Therefore the reliability of the $u^* - r^*$ color criterion for selecting spectroscopic early types is 83%. The *completeness* is defined as the fraction of all galaxies of a given type from the original sample that are selected by the classification scheme. The $u^* - r^* \geqslant 2.22$ color selection criterion for early types selects 284 of the 290 early-type galaxies from the spectroscopic sample, resulting in a completeness of 98%.

Based on the brighter morphological sample, $C > 2.63$ and $C < 2.63$ give equally complete ($\sim 83\%$) subsamples of early- and late-types of galaxies, with 76% reliability for the early- and 88% reliability for the late-type selection. Equal reliability (81%) for the selection of early and late types is given by a $C = 2.83$ separator, with completeness of 70% and 80% of the early and late subsamples, respectively. Based on the spectroscopic sample, $C > 2.55$ and $C < 2.55$ give equally complete ($\sim 73\%$) subsamples of early and late types of galaxies, with 78% reliability for the early- and 66% for the late-type selection. Equal reliability (72%) for the early- and late-type selection is given by a $C = 2.40$ separator, with completeness of 85% and 54% for the early- and late-subsamples, respectively. We adopt a $C = 2.6$ separator, which is optimized for completeness of subsamples selected from both the spectroscopic and morphological samples and gives equally reliable types in both. Shimasaku et al. (2001) recommend a different separator for an early-to-late cut at S0/Sa. They suggest an inverse concentration index of 0.33 ($C \sim 3$), based on a bright sample of 456 galaxies, optimized for low contamination. The different definition of the cut and its optimization make direct comparison with our results difficult.

The correlation of the concentration index and $u^* - r^*$ color is illustrated in Figure 8 (*right*), where a $g^* < 20$ subsample is given as contours and the spectroscopic sample as points. The limit of $g^* = 20$ for the galaxy subsample in Figure 8 was chosen to ensure low contamination and a higher fraction of red galaxies.

3.3. *Comparison of Morphology Selection Criteria*

The selection criteria for early- and late-type galaxies are compared in Tables 2 and 3 against the spectroscopic and visual classification, respectively. The upper part of the tables compares selection methods for early-type galaxies, while the lower part compares selection methods for late-type galaxies. From Table 2, based on the spectroscopic classification, all selection criteria have comparable reli-

TABLE 2

COMPARISON BETWEEN CLASSIFICATION METHODS FOR THE SPECTROSCOPIC SAMPLE

Selection Rule	Completeness	Reliability
$u^* - r^* \geqslant 2.22$	98%	83%
$P_{\mathrm{deV}} > P_{\exp}$	96%	76%
$C > 2.6$	68%	81%
$u^* - r^* < 2.22$	72%	96%
$P_{\exp} > P_{\mathrm{deV}}$	55%	90%
$C < 2.6$	77%	64%

NOTE.—The exponential and de Voucouleurs law likelihoods and the radii used in computing the concentration index are all measured in the r^* band.

TABLE 3

COMPARISON BETWEEN CLASSIFICATION METHODS FOR THE MORPHOLOGICAL SAMPLE

Selection Rule	Completeness	Reliability
$u^* - r^* \geqslant 2.22$	80%	62%
$P_{\mathrm{deV}} > P_{\exp}$	99%	42%
$C > 2.6$	84%	75%
$u^* - r^* < 2.22$	66%	83%
$P_{\exp} > P_{\mathrm{deV}}$	6%	91%
$C < 2.6$	81%	88%

ability for selecting early types, but the concentration index selection method is only $\sim 68\%$ complete, compared with more than 95% completeness of the profile likelihood and color selection methods. The color selection method is preferable in choosing subsamples of late-type galaxies, with $\sim 72\%$ completeness and $\sim 96\%$ reliability. The profile likelihood method for late-type selection misses almost half of all late-type galaxies, while the concentration index criterion is only $\sim 64\%$ reliable.

Table 3 gives analogous results based on the visual classification of the bright ($g^* < 16$) morphological sample. The performance of the concentration index criterion for this bright galaxy sample is comparable to that for the spectroscopic sample, with increased reliability for selecting early- (from 68% to 84%) and late-type (from 73% to 85%) galaxies. The profile likelihood criterion has severe problems for very bright galaxies, missing 94% of the spirals present in this sample (see the Appendix). For the bright morphological sample, the color criterion is less complete and less reliable for both early- and late-type selection than the concentration index method.

Unfortunately, the color, concentration index and profile likelihoods criteria can be compared with independent morphological classification only at the bright end. Beyond $g^* \sim 18.5$ (which roughly corresponds to the spectroscopic limit of $r^*_{\mathrm{petro}} < 17.8$), we are forced to compare the different methods between themselves. The correlation between color and concentration index gets weaker for fainter magnitude samples, as illustrated in Figure 9 (*right*). In the spectroscopic sample, only 10% of the galaxies with higher concentration index characteristic of early types ($C > 2.6$) have colors bluer than $u^* - r^* = 2.22$. For $17 < g^* \leq 19$ in the photometric sample, 18% of $C > 2.6$ galaxies have blue colors, with the percentage increasing to 26% and 43% for $19 < g^* \leq 20$ and $20 < g^* \leq 21$, respectively. When we impose a more stringent cut for selecting early types, requiring both $C > 2.6$ and $P_{\mathrm{deV}} > P_{\exp}$, for $17 < g^* \leq 19$ we reduce the number of selected galaxies by $\sim 13\%$, and the fraction of blue galaxies among those selected to 13%. For $19 < g^* \leq 20$ and $20 < g^* \leq 21$, 20% and 36% fewer galaxies are selected, and the blue fraction is reduced to 17% and 26%, respectively. Since we expect no more than 75% to 81% reliability even at the bright end for early-type selection based on the concentration index criterion alone, we do not expect the contamination to be much less than $\sim 20\%$. It is therefore likely that by using the concentration index criterion alone to select early types, we are including an extra 10% to 20% of late types for $19 < g^* \leq 20$ and $20 < g^* \leq 21$, respectively.

A similar trend of weakening of the correlation between profile likelihoods and $u^* - r^*$ color for faint galaxies is also observed (Fig. 9, *left*). For $g^* > 19$ there is an increasing
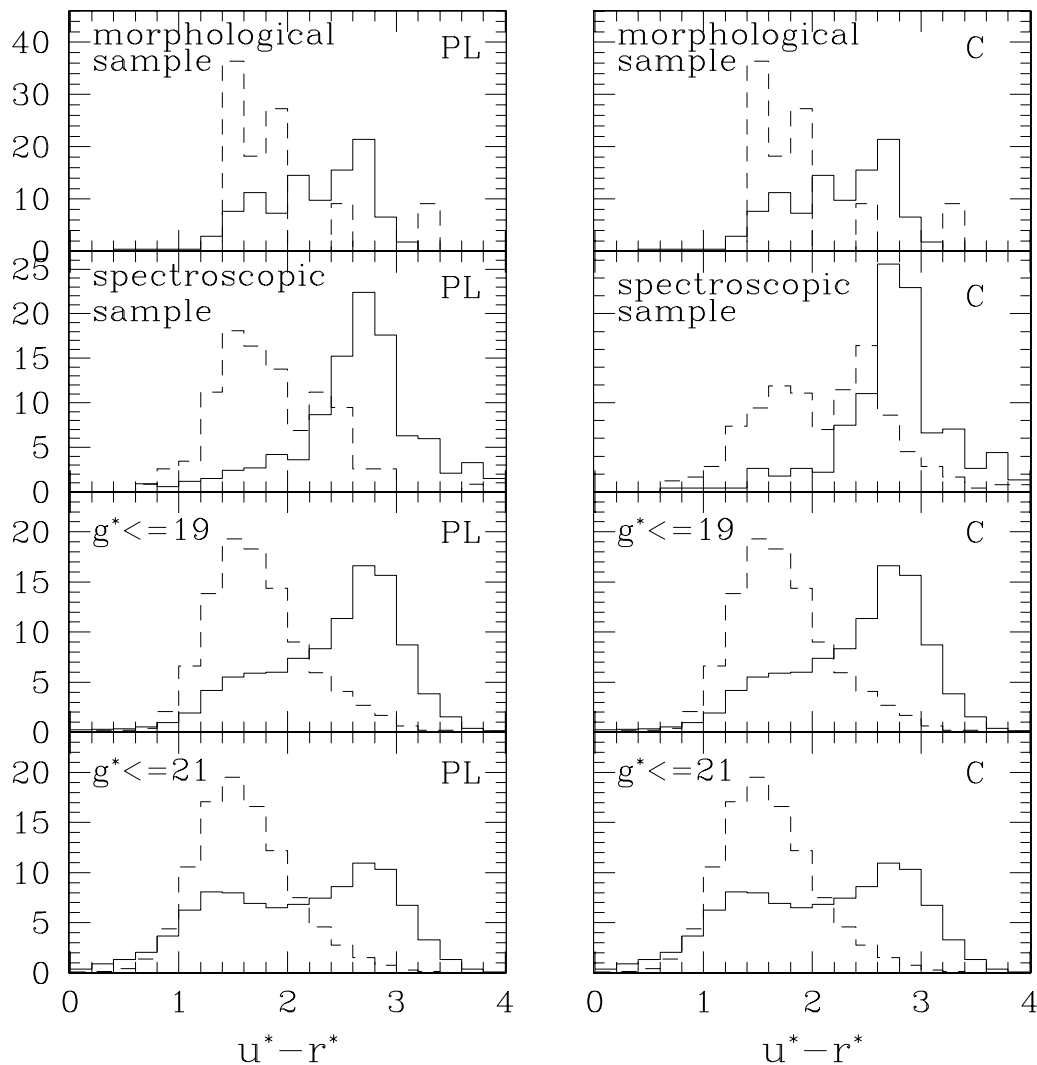
Fig. 9.—Color histograms $u^* - r^*$ of early-type (*solid lines*) and late-type (*dashed lines*) galaxies selected using the profile likelihood (*left*) and concentration index (*right*) criteria.

fraction of galaxies that are better fitted by a de Vaucouleurs' profile and have blue colors $u^* - r^* < 2.22$. For $20 < g^* < 21$, this fraction increases to 43% of all $P_{\rm deV} > P_{\rm exp}$ galaxies, from $\sim 30\%$ for brighter magnitudes. The profile likelihood criterion is less discriminative for early-type selection than either the concentration index or $u^* - r^*$ color criteria, at both bright and faint magnitudes. Comparing the numbers of galaxies selected as early types by $P_{\rm deV} > P_{\rm exp}$ alone with those selected by both $C > 2.6$ and $P_{\rm deV} > P_{\rm exp}$, we find that only 57% ($17 < g^* \leq 19$), 48% ($19 < g^* \leq 20$), and 41% ($19 < g^* \leq 20$) are "confirmed" by the concentration index cut. Thus both concentration index and color of faint galaxies seem to suggest that the profile likelihood method for selecting early types includes as much as an extra 50% to 60% late-type galaxies at the faint end ($19 < g^* \leq 21$).

Since we do not expect appreciable evolution in the colors of early- and late-type galaxies and theoretical population synthesis studies suggest that $u^* - r^*$ color remains a good discriminator over the redshift range considered ($z \leq 0.4$), we are inclined to believe that the profile likelihood and concentration index method, which rely on spatial information hard to obtain at the faint end, fail before the color criterion does. The discrepancies between

the three methods for faint magnitudes, quantified above, support that view.

Overall, the concentration index criterion an be used at the very bright end ($g^* < 16$), where galaxies are also easy to classify both visually and spectroscopically. The profile likelihood criterion is currently applicable to galaxies at intermediate magnitudes ($16 < g^* < 18$), with a somewhat low completeness for late-type selection and low reliability for early-type selection. In this range the concentration index and color criteria both give better results. The color criterion is applicable for all magnitude ranges considered, and we specifically recommend its use for fainter samples ($g^* > 18$).

4. CONCLUSIONS

This study indicates that galaxies have a bimodal $u^* - r^*$ color distribution corresponding to early (E, S0, and Sa) and late (Sb, Sc, and Irr) morphological types, which can be clearly separated by a $u^* - r^*$ color cut of 2.22, independent of magnitude. The peak-to-peak width of this $u^* - r^*$ color separation is $\gtrsim 1.1$ mag, about twice as large as the sum in quadrature of the widths of each peak (where the width includes both color errors and the intrinsic color dispersion), even for the faintest magnitudes considered

($g^* \lesssim 21$). As can be seen from Figures 1 and 3, other color combinations ($r^* - i^*$, $i^* - z^*$, $g^* - r^*$, and $u^* - g^*$) have much smaller peak-to-peak separations between the two populations. The SDSS $u - r$ color is a unique combination of an ultraviolet u band bluer than the Johnson-Morgan U band [$\lambda_{eff}(u) = 3543$ Å versus $\lambda_{eff}(U) = 3652$ Å] and a broader and redder r band ($\lambda_{eff} = 6231$ Å, FWHM = 1373 Å) compared with Johnson-Morgan V ($\lambda_{eff} = 5505$ Å, FWHM = 827 Å), allowing for a more sensitive comparison of the blue and red portions of the galaxy spectra, relevant for isolating star formation rates. The u^* and r^* filters always bracket the Balmer break, and the theoretical tracks of galaxy color evolution with redshift in the $u^* - g^*$ versus $g^* - r^*$ color-color diagram are parallel to the $u^* - r^* = \text{const}$ lines up to $z \sim 0.4$, supporting the claim that this separation is applicable to samples at all redshifts relevant for the main sample of SDSS galaxies. We find evidence for the evolution of the $u^* - r^*$ color distribution with fainter magnitudes, indicative of the presence of larger fractions of bluer galaxies at redshifts of $z \sim 0.4$.

Among the SDSS parameters calculated automatically by the photometric pipeline PHOTO, concentration indices and profile likelihoods are also sensitive to morphology and correlate with $u^* - r^*$ color. Unlike the concentration index and profile likelihood methods, the $u^* - r^*$ color separation does not require well-resolved images.

Since star formation rate is one of the defining characteristics of the Hubble sequence, it is expected that $u^* - r^*$ color, as an indicator of recent star formation, correlates with Hubble type. Other defining parameters for the Hubble types are the bulge-to-disk (B/D) ratio and the tightness of the spiral pattern. Those three parameters can be effectively reduced to two underlying ones—the star formation history and the mass distribution of the galaxy. The B/D ratio, the concentration index, and the profile likelihoods are just three ways of measuring the mass distribution using the stellar light, while the tightness of the spiral pattern is presumably dependent on the mass distribution, as well as recent star formation. Moreover, the mass distribution and star formation are probably not strictly independent; for example, we found correlations between the color as a measure of star formation, and the concentration index and the profile likelihoods as measures of the mass distribution. In view of this dependence of Hubble types on two underlying internal (as opposed to environmental) parameters, it is not surprising to see that neither of the measures we use gives a perfect correspondence to morphology. The $u^* - r^*$ color, concentration index, and profile likelihoods, as independent, quantitative indicators of morphology, are more accessible and less subjective than Hubble types and are thus more beneficial to the studies of galaxy properties and formation.

APPENDIX A

MODEL QUANTITIES

The optimal measure of the total flux associated with an object is the result of the convolution of the image with a matched filter. Even if the matched filter used is not an accurate representation of the shape of the object, this gives an unbiased measure of the color of the object if the same matched filter is used in each band. With this in mind, the SDSS PHOTO pipeline performs three model fits to each object in every band: a point-spread function (PSF), a pure de Vaucouleurs profile, and an exponential disk; the galaxy models are convolved with the local PSF. In each case, the fit is done to the two-dimensional data, and the galaxy models allow for an arbitrary scale length, axial ratio, and position angle. These fits are carried out by minimizing χ^2, not over each pixel (which would be terribly time-consuming) but over a series of *sectors*, which divide the image into radial and angular bins (Lupton et al. 2001). An error is associated with the flux in each sector, based on photon statistics and the measured pixel variance within the sector. Galaxy colors are measured by applying the best-fit model of an object in the r band to the other bands, thus measuring the flux through the same effective aperture.

Of course, real galaxies do not necessarily follow pure exponential or de Vaucouleurs profiles: they have composite profiles, spiral arms, and other features not included in these models. Thus the likelihoods of the model fits tend to be low for well-resolved, high signal-to-noise ratio galaxies, and the likelihood ratio of exponential and de Vaucouleurs fits is a poor measure of morphology. Moreover, the version of PHOTO used in these reductions weighs strongly the inner parts of galaxies while performing the profile fits, which overestimates the contribution of the de Vaucouleurs bulge. Work is ongoing to include model uncertainties in the error associated with the photometry in each sector in PHOTO, which should make these fits more meaningful at the bright end.

The model flux is calculated by integrating all the light under the best-fit profile and consequently is not equal to the Petrosian flux for a given galaxy. A comparison between model and Petrosian magnitudes in the u^* and r^* bands and $u^* - r^*$ color is given in Figure 10. The majority of galaxies are enclosed in linearly spaced, isodensity contours, with the outliers shown as points. At the faint end ($u^* > 19$
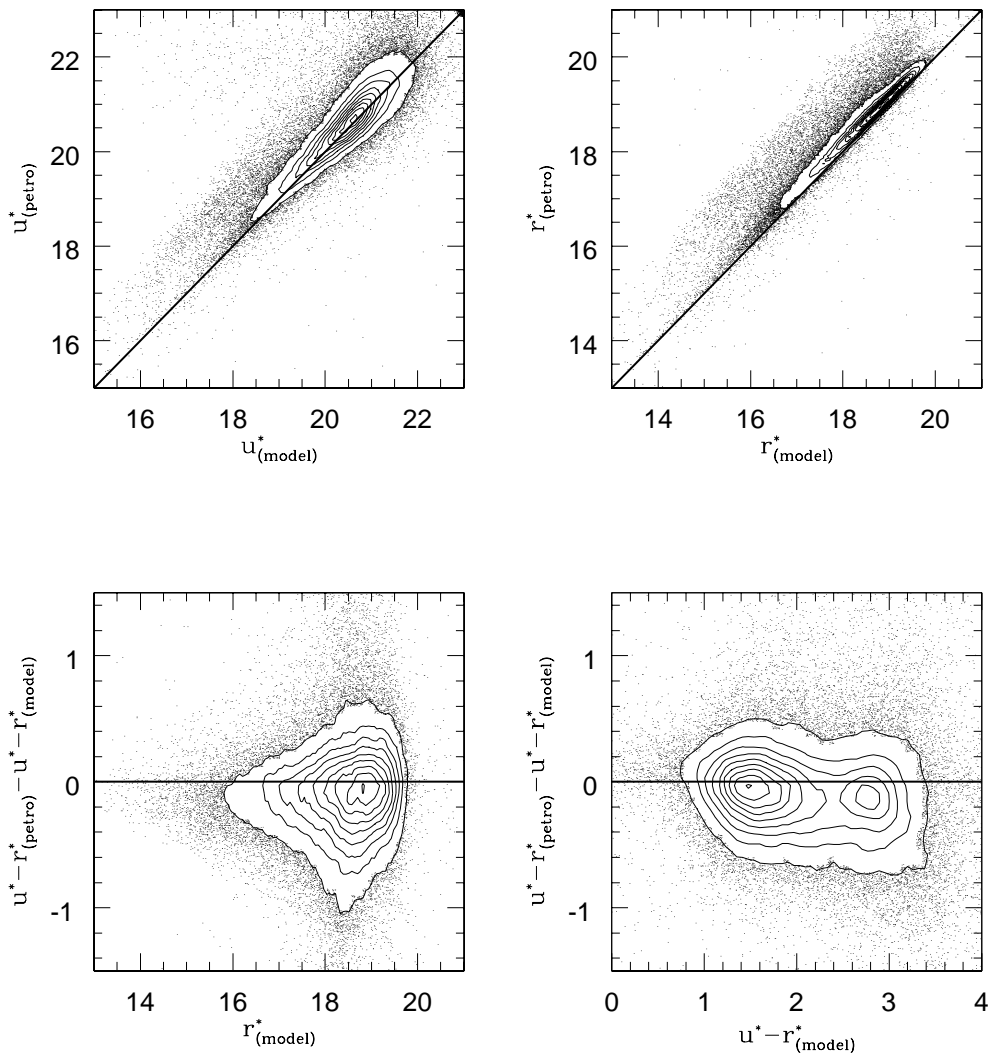

FIG. 10.—Model and Petrosian magnitudes. The contour curves are linearly spaced isodensity curves; the outliers are shown as points. *Top left*, u^*_{model} vs. u^*_{petro}; *top right*, r^*_{model} vs. r^*_{petro}; *bottom*, difference between Petrosian and model $u^* - r^*$ color as a function of r^*_{model} magnitude (*left*) and $(u^* - r^*)_{model}$ color (*right*). For more details see the Appendix.

and $r^* > 16$), the model and Petrosian magnitudes in u^* (*left*) and r^* (*right*) are almost identical, with the majority of galaxies lying close to the model-equals-Petrosian magnitude line. At the bright end, however, a large fraction of the galaxies have fainter Petrosian magnitudes by as much as 1 mag. Those are galaxies better fitted by the de Vaucouleurs profile for which the Petrosian flux is not equal to the total flux. Figure 10 (*bottom*) shows the difference in $u^* - r^*$ color measured using the model and Petrosian magnitudes as a function of model magnitude and model $u^* - r^*$ color. The value of $u^* - r^*_{petro}$ is ~ 0.15 mag bluer than $u^* - r^*_{model}$, with the difference being more pronounced for ellipticals than spirals (*bottom right*). As pointed out by Yasuda et al. (2001), the model fits are heavily weighted toward the bright cores of galaxies and thus de-emphasize the bluer disk component of ordinary spiral galaxies. This is consistent with a somewhat redder model than Petrosian colors.

REFERENCES

Bernardi, M., et al. 2001, in preparation
Blanton, M., et al. 2001, AJ, 121, 2358
Brown, M. J. I., Webster, R. L., & Boyle, B. J. 2000, MNRAS, 317, 782
Buta, R., & Williams, K. L. 1995, AJ, 109, 543
Cheeseman, P., & Stutz, J. 1996, in Advances in Knowledge Discovery and Data Mining, ed. U. M. Fayyad, G. Piatetsky-Shapiro, P. Smyth, & R. Uthurusamy (Cambridge: AAAI Press/MIT Press), 63
Connolly, A., et al. 2001, ApJ, submitted
de Vaucouleurs, G. 1961, ApJS, 5, 233
Dodelson, S., et al. 2001, ApJ, submitted
Eisenstein, D., et al. 2001, AJ, submitted
Fan, X. 1999, AJ, 117, 2528
Fan, X., et al. 1999, AJ, 118, 1
Ferreras, I., Cayon, L., Martinez-Gonzalez, E., & Benitez, N. 1999, MNRAS, 304, 319

Finlator, K., et al. 2000, AJ, 120, 2615
Fioc, M., & Rocca-Volmerange, B. 1997, A&A, 326, 950
———. 1999, A&A, 351, 869
Fischer, P., et al. 2000, AJ, 120, 1198
Fukugita, M., Ichikawa, T., Gunn, J. E., Doi, M., Shimasaku, K., & Schneider, D. P. 1996, AJ, 111, 1748
Fukugita, M., Shimasaku, K., & Ichikawa, T. 1995, PASP, 107, 945
Goebel, J., Stutz, J., Volk, K., Walker, H., Gerbault, F., Self, M., Taylor, W., & Cheeseman, P. 1989, A&A, 222, L5
Gunn, J. E., et al. 1998, AJ, 116, 3040
Hanson, R., Stutz, J., & Cheeseman, P. 1999, Bayesian Classification Theory (Technical Report FIA-90-12-7-01) (Moffett Field, CA: NASA Ames Research Center, Artificial Intelligence Branch)
Hubble, E. 1936, The Realm of the Nebulae (Oxford: Oxford University Press)

Humason, M. L. 1936, ApJ, 83, 10
Ivezić, Ž., & Elitzur, M. 2000, ApJ, 534, L93
Kennicutt, R. C. 1992, ApJS, 79, 255
Kochaneck, C. S., Pahre, M. A., & Falco, E. E. 2000, preprint (astro-ph/0011458)
Lupton, R. H., Gunn, J. E., & Szalay, A. 1999, AJ, 118, 1406
Lupton, R. H., et al. 2001, in preparation
Morgan, W. W., & Mayall, N. U. 1957, PASP, 69, 409
Oke, J. B., & Gunn, J. E. 1983, ApJ, 266, 713

Schlegel, D., Finkbeiner, D. P., & Davis, M. 1998, ApJ, 500, 525
Shimasaku, K., et al. 2001, AJ, 1238
Stoughton, C., et al. 2001, in preparation
Strauss, M., et al. 2001, in preparation
Szalay, A., et al. 2001, AJ, submitted
Tegmark, M., et al. 2001, ApJ, submitted
Yasuda, N., et al. 2001, AJ, in press
York, D. G., et al. 2000, AJ, 120, 1579
Zehavi, I., et al. 2001, ApJ, submitted